

# Opto-mechanical review of a light weight compact visible zoom camera

Brian McMaster

Corning Tropel, 60 O'Connor Road, Fairport, NY, USA, 14450

## ABSTRACT

An overview of a high performance zoom camera will be presented. Performance achievements including zoom (magnification range), mass, bore sight, space envelope and environment will be discussed. Optical mounting techniques and flexural decoupling of components for large temperature ranges will be presented. Precision trajectory and positioning of multiple moving lens groups will be reviewed and lead screw decoupling methods providing axial stiffness with radial compliance will be illustrated. A mechanical system interface with high stiffness and thermal compliance for azimuth and elevation adjustments will be given. Finally, the paper will conclude with a review of lessons learned, including lead screw decoupling and aligning multiple static and moving lens groups.

**Keywords:** Zoom Camera, Flexure, bore sight, lead screw, mechanical stiffness, thermal compliance.

## 1. INTRODUCTION

The mechanical design of this lens was driven by customer specified optical design (telephoto) and a solid model based space envelope. The main focus of this paper is how the mechanical systems met the requirements that the optical design demanded. While the actual optical prescription will not be discussed, top level optical parameters will be included where applicable.

In order to meet the demands that the optical prescription required, a host of mechanical concepts were identified taking examples from many different industries and evaluated to determine if each had the potential to solve a particular need. These were then down selected using analysis results and experimental data generated by prototypes to the lens described in this paper.

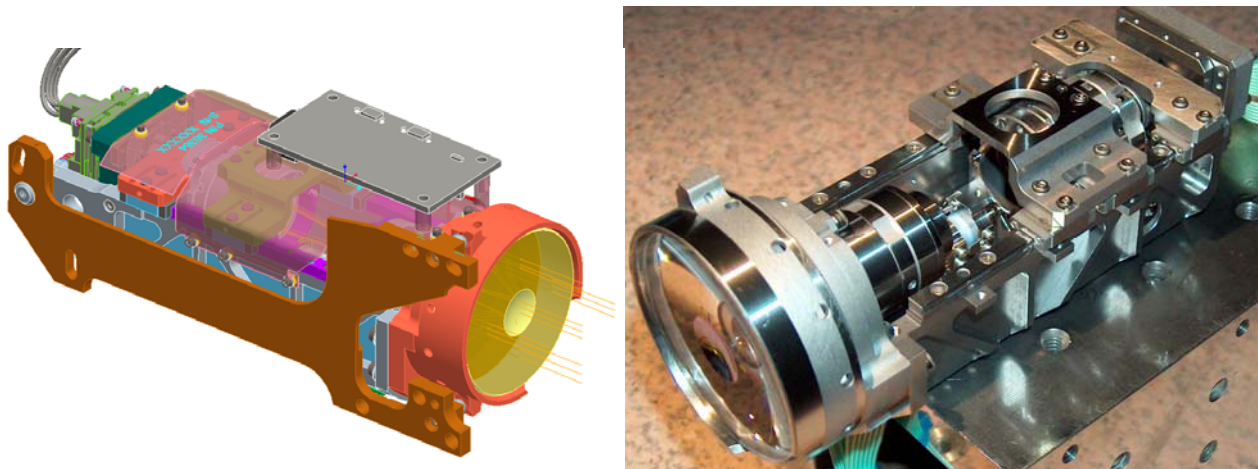


Fig. 1. The visible spectrum lens described in this paper. It has a focal length range of 130mm to 650mm. The input aperture is 57mm and the OAL is 185 mm. The brown plate shown is the primary mechanical interface for mounting to the customer support structure.

## 2. ACHIEVEMENTS FOR THE MECHANICAL SYSTEMS

Using optical analysis methods, mechanical performance needs were generated for the top level and several subsystems of the lens. These were used to down select the mechanical concepts to integrate into the final design. The table below illustrates the noteworthy parameters achieved by the mechanical subsystems:

Table 1. Optical and Mechanical Parameters achieved by the lens system:

| Parameter Description                               | Achieved Value                      |
|---|-------------------------------------|
| Bore sight stability                                | 150 $\mu$ Rad                       |
| Bore sight repeatability                            | 31 $\mu$ Rad                        |
| Static/dynamic group perp.                          | 7 microns                           |
| Moving group alignment                              | 2 - 5 microns                       |
| Moving group trajectory                             | 1.0 micron                          |
| Moving group axial position resolution (lead screw) | 2.0 micron                          |
| Air space tolerance on static elements              | 1 to 5 microns                      |
| Total mass  | 1.3 kg                              |
| Operating temp. range*                              | -25 $^{\circ}$ C to 71 $^{\circ}$ C |
| First resonance frequency.                          | 625 Hz.                             |

\* This is the temperature range the mechanical systems operated over.

Tolerance budgets were generated using these numbers that took into account factors such as fabrication, alignment, thermal and lead screw tolerances.

## 3. SYSTEM BORE SIGHT STABILITY

In order to meet not only optical but thermal, schedule and cost requirements, a homogeneous material design was employed. This allowed the use of commercially available bearings (but not lead screws) to be mounted directly to the lens chassis. As some of the materials were not disclosed by the vendors, experimental methods were used to ensure that CTE mismatches were avoided.

However, the customer support structure was based on aluminum. This required lens mounting plate to also be aluminum and the use of a decoupling design for the mechanical connection to the lens chassis (stainless steel). Due to the difference in CTE between the metals, length and storage temperature range, a 0.17 mm length difference between the aluminum customer support structure and the steel lens chassis is generated.

Furthermore, the dynamic stability requirement required a high resonance frequency. Several flexure based designs were investigated and analyzed. None were able to meet the vibration stiffness requirements and allow for the thermal compliance needed to maintain bore sight stability and repeatability over the storage temperature range.

Therefore, a 3ball/3Vee design with co-axial fasteners was employed. This met the stiffness needs and with careful attention to contact stress and coefficient of friction, also met the thermal compliance needs. FEA analysis was

performed based on the calculated friction forces to determine if deformation of the Chassis would exceed the optical based requirements.

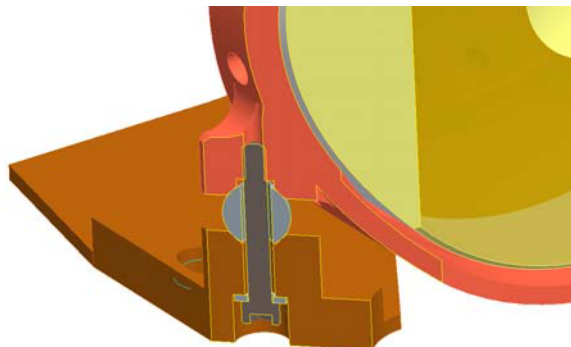


Fig. 2. Cross Section of front ball/Vee interface. The ball is fixated via a cone in the brown aluminum mounting plate and the Vee axis is normal to the section plane. The Vee is milled into the salmon colored steel part.

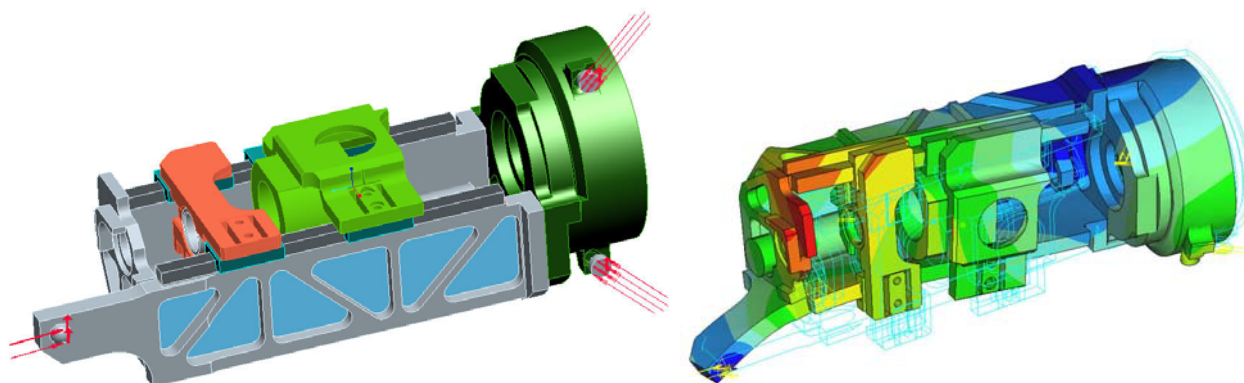


Fig. 3. A view of the applied friction loads due to preloading the balls into its respective vee and resulting structural deformation. Max compression von Mises contact stress was used to calculate frictional forces between the balls and vees. The max image bore sight due to de-center of the moving and non moving groups was 38microns worst case.

Further investigation was also performed with respect to deformation of the optical surfaces due to this CTE miss match between the lens and the lens mount. Using the above frictional loads, a NASTRAN model was generated to determine the severity of deformation of the first optical element in the system when the steel mount is deformed with the frictional loads. Zernike polynomials were generated from the deformed FEA model, and then imported into CODE V® for image degradation analysis. Image quality degradation did not exceed specified limits.

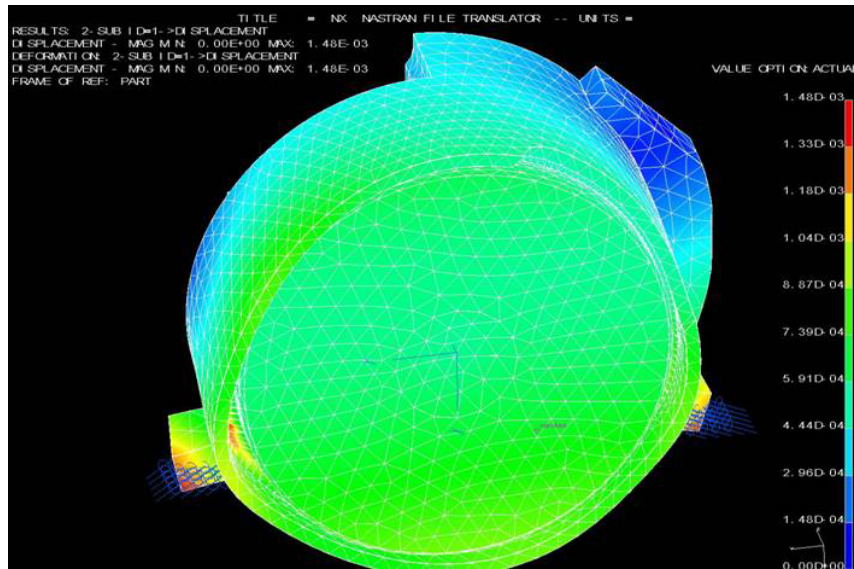


Fig. 4. NASTRAN model using parabolic tetrahedrons for the first optical element and its cell. The four unique optical surfaces had Zernike polynomials fit to the deformed surface and imported into CODE V® for image degradation evaluation.

#### 4. MOVING GROUP TRAJECTORY

The mechanical system design used a split approach, separating the static group from the two moving groups. Using a common datum, the assemblies can be aligned separately with different alignment techniques. This common datum was also used for referencing not only the optical surfaces but also for referencing the trajectory of the two moving bridge structures that held the two lens groups.

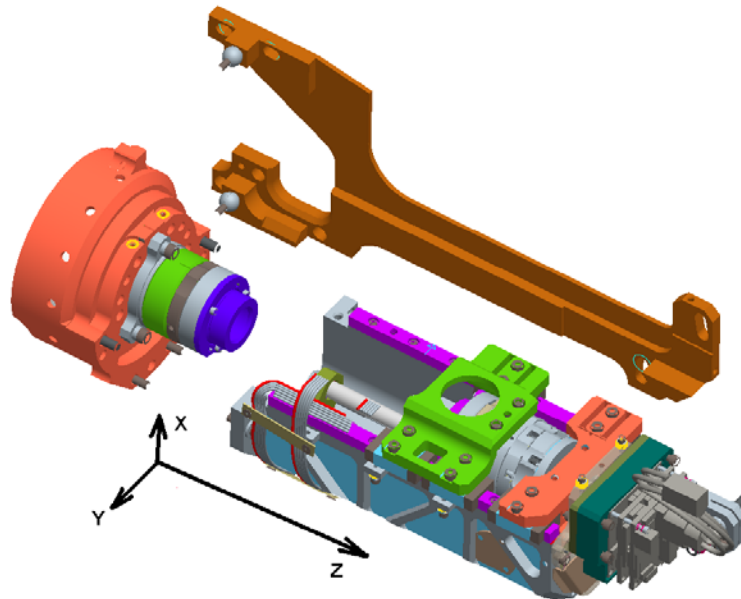


Fig. 5. Exploded view of the two main sections of the lens and the mounting interface plate, covers removed. The round section contains the static group including the smaller diameter optical stack. The green bridge suspends the first moving group and the salmon bridge next to it suspends the second moving group.

Each of the two moving groups had a 6 micron de-center requirement of which 4 were used by the lens group alignment and fabrication tolerances. Thus, the trajectory of the two moving groups required a 2 micron maximum de-center. This was achieved by precision grinding the bearing rail mounting surface and grinding the common datum perpendicular to the rail mounting surface. This still left the Y axis alignment to be performed by manually deforming the bearing rails to achieve the straight line motion required in the Y axis.

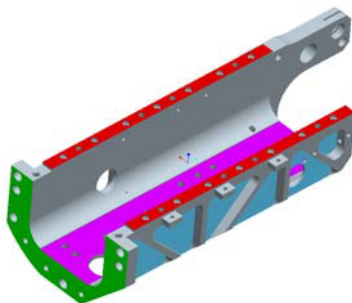


Fig. 6. Flatness and perpendicularity were precision ground into the part called the "channel". The red surface determines the X axis de-center. It was ground to less than 1 micron flatness. The green surface was ground to less than one micron perpendicularity to the red surface. The green surface was used for the trajectory alignment reference as well as the common datum to mate with the static group.

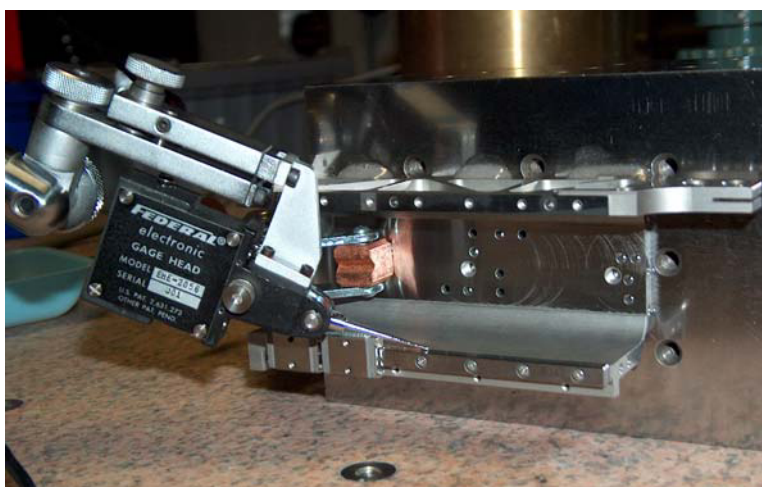


Fig. 7. Alignment of the remaining slider bearing axis not controlled by machining tolerances. Manual tapping and tightening of fasteners was used to achieve 1 micron alignment over the length of the bearing rail.

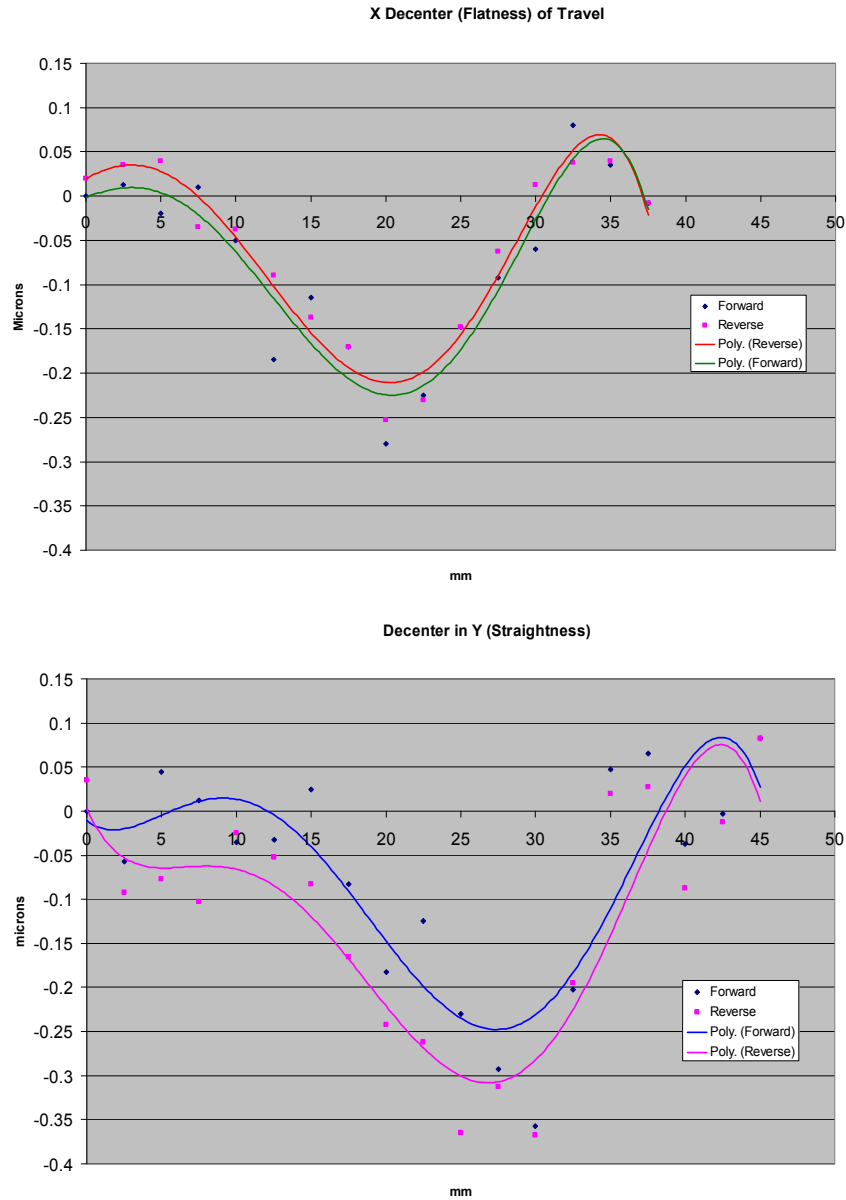


Fig. 8. The resulting trajectory in de-center significantly outperformed the 1micron requirement. The X de-center is mainly dependent on bearing running parallelism and mounting surface flatness. The Y de-center is highly dependent on the manual alignment of the bearing rail to the perpendicular datum plane to the flatness of the bearing rail mounting surface. Future efforts will rely on precision fixtures for this effort.

Both pitch and yaw measurements were within the +/- 15 arc seconds requirements. No discernable pattern was observed. This was attributed to friction in the bearings and was not investigated further.

## 5. LEAD SCREW DECOUPLING

The method for positioning the lens groups employed a DC servo motor with an integrated gear head driving a multi beam flexural coupling connected to a lead screw/nut for each lens group. The length of the screw was preloaded axially on the end opposite the motor with a compressible washer loaded to always keep the screw in tension during vibration and thermal cycles. Due to fabrication tolerances, assembly techniques, thermal gradients, etc. the lead screw was decoupled from the lens moving groups so as to not affect the trajectory quality by “pulling” the moving lens group off axis.

The required connection stiffness between the nut and the lens moving group to prevent “pulling” yet ensure proper lens position along Z is in the Z and in  $\theta Z$  (torque) axis. The final design accomplished these two stiff connections but also possessed an undesired additional stiffness in  $\theta X$ .

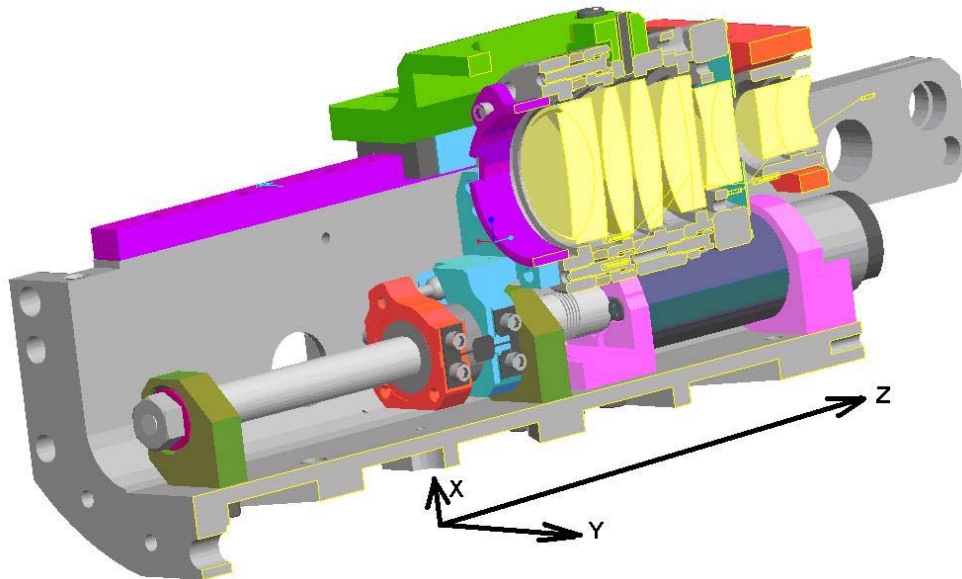


Fig. 9. Sectional view of both moving groups with the motor/lead screw drive for just moving group1. Pillow blocks are shown in green, the lead screw nut is orange. The flexures decouple the orange nut from the blue part which is rigidly mounted to the lens moving group.

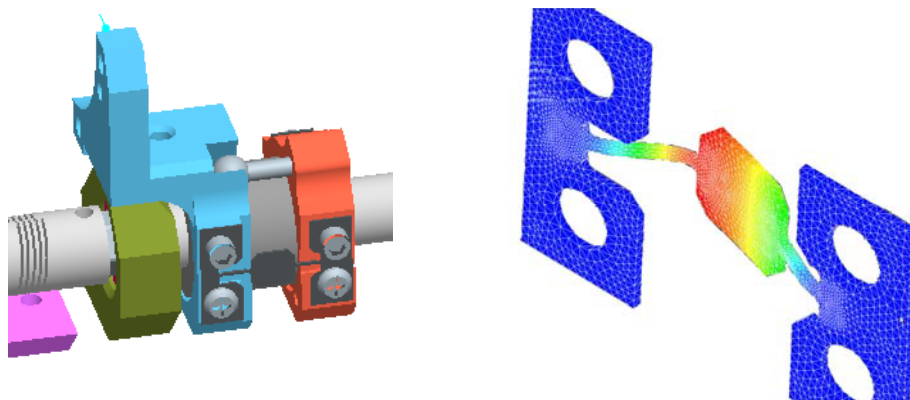


Fig. 10. Close up of the decoupling flexure (stiffness in Z) and NASTRAN model for buckling of the flexure. The analysis indicated a buckling safety factor of 4 with this geometry.

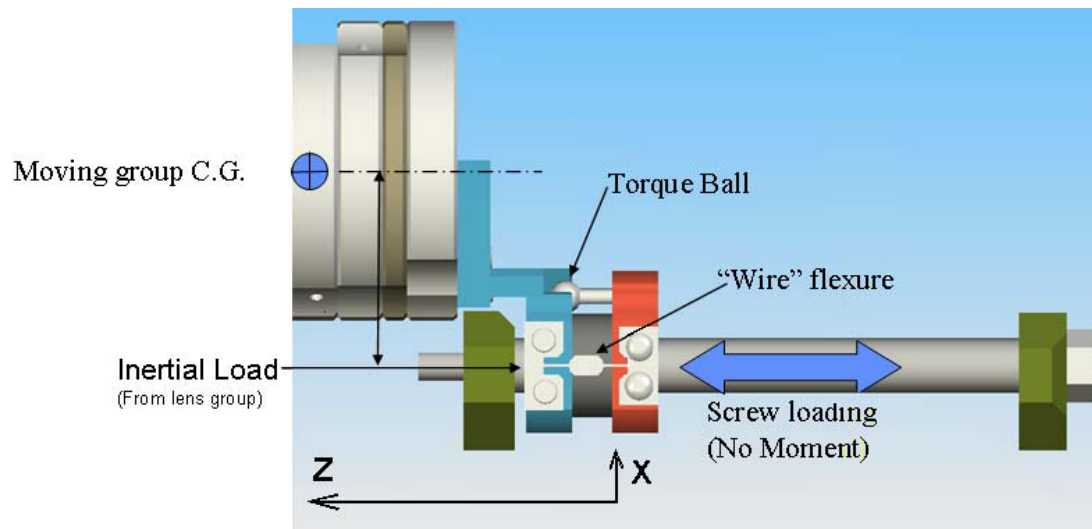


Fig. 11. Details of the load path for the lead screw decoupling design.

The “wire” flexure geometry was driven by buckling loads, XY& $\theta$ Y plane compliance, cost and ease of assembly. To minimize the trajectory degradation, the XY stiffness of the moving group was measured and compared to the force expected by the pull of the lead screw nut through the flexures. The buckling load was determined by the maximum specified acceleration of the lens coupled with the mass of the moving group. The manufacturing method chosen was chemical etching of flat stock from both sides, thus producing the desired radii on the stressed edges.

The undesired stiffness  $\theta$ X was mitigated by precision alignment of the lead screw rotational axis to the moving group trajectory axis. The pillow block mounting screw holes (in the purple surface in fig. 7) provided the adjustment to accomplish the alignment between the lead screw and moving group. The alignment method used was similar to the method shown in fig. 8.

## 6. LESSONS LEARNED

### 6.1 Moment loading of the lead screw nut.

The first version of the lead screw decoupling design loaded the nut off axis. Under vibration, this created a  $\theta Y$  moment on the nut allowing the moving lens group excessive “slop”. In hind sight, proper attention to load path (dynamic and static) would have foreseen this difficulty. It was discovered by simulating dynamic loading by applying a fixed external static load to the moving group and observing the effect on magnification and focus.

Lesson Learned: Know your load path and FEA can only go so far.

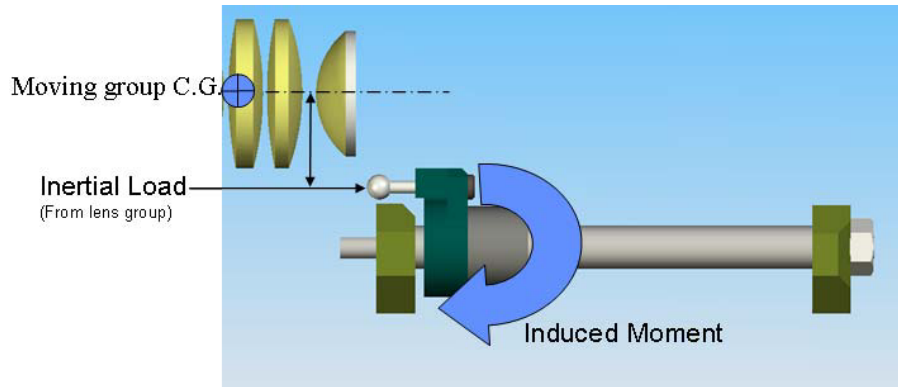


Fig. 12. The “ball on a stick” design coupled the displacement of the nut to a vee mounted on the lens moving group. While providing the required stiffness and freedoms, excessive hysteresis occurred during dynamic load simulations. This was due to the thread interface between the nut and the threads on the lead screw

### 6.2 Dynamic range of alignment equipment.

While approaching final alignment of this assembly, alignment of a particularly fast surface (6mm radius of curvature lens surface) proved to be near impossible. A non-rotationally symmetric mount and very limited access prompted the selection of an interferometer type alignment method. However, in practice, the limited dynamic range of this method required near perfect alignment for any feedback whatsoever. After much creative alignment and transfer of data, an alternate method was employed.

Lesson Learned: Selection of alignments methods needs to include more than resolution, accuracy and access. Do not overlook dynamic range.

### 6.3 Usage Models.

A light press fit & adhesive was used to mount the thrust bearing on each of the lead screws. During testing, this joint failed and the two parts separated. All the static tests performed could not duplicate the failure. Upon further investigation, fatigue loading of the adhesive was identified as the root cause of the failure of the joint. A seemingly unrelated test included mechanical end of travel contact creating high thrust loads on the adhesive. The initial testing did perform a statistically significant sample size to induce this fatigue failure.

Lessons Learned: Know your customer’s usage model. Adhesives can be very poor in fatigue.

#### 6.4 Environmental (thermal) chambers, humidity and optics.

During the environmental testing of a prototype of this lens, it was placed in a thermal chamber to evaluate bore sight changes over temperature. After successfully measuring bore sight at  $-35^{\circ}\text{C}$ , the chamber was powered down and left to warm back to room temperature. The following day, the chamber was opened to discover that room air had infiltrated the chamber prior to coming up to ambient temperature. The water in the room air condensed on the cold surfaces resulting in large volumes of water collecting inside the prototype lens and surrounding areas. While the lens was not rated to operate in a condensing environment, no permanent damage occurred.

Lesson Learned: Use the thermal chamber to maintain humidity control while returning from cold to room temperatures.

#### 6.5 Motor Controllers.

Several issues regarding motor controllers arose during this project. The main issues revolved around using different controllers & amplifiers at Corning Tropol versus the equipment and homing algorithms used by the end user.

Lesson Learned: All motion parameters should be identified at the beginning of a project and must be periodically reviewed and confirmed up to and including integration. These parameters should include maximum velocity & acceleration, voltage & current, fault tolerance and detection, homing algorithms, PWM (including freq.) vs. linear amplifiers, etc.

## 7. CONCLUSIONS

The success of this lens meeting all performance requirements was due to several factors. Namely, extensive analysis that drove tolerance budgets, extensive testing (optical, mechanical and environmental) and having ultra precision tooling and manufacturing technology in house. This allows the design of a system or component to be closely coupled to the process chosen to fabricate it. Furthermore, unforeseen problems can be quickly resolved by exploiting any additional precision inherent in the part or system fabrication.



Fig. 13. Smoke stack image. This object was 0.9km (0.6 miles) away from Corning Tropol.